Research Square

Preprints are preliminary reports that have not undergone peer review.
They should not be considered conclusive, used to inform clinical practice,
or referenced by the media as validated information.

Construction of Waterborne Polyurethane Composites via Phytate-Chitosan-Modied Boron Nitride and DOPO Derivative Synergy: A route to flame retardancy and multifunctional performance

Yanling Yue
Guiyang University
Bingyue Huang
Guiyang University
Deyu Liu
Guiyang University
Shaoyuan Wu
Guiyang University
Jinghan Hu
Guiyang University
Shiyi Ming
Guiyang University
Xingyu Guan
Guiyang University
Yi Zhang
Guiyang University
Kui Wang
Guiyang University
Weijiang Huang
Guiyang University
Wei Yan
yw2410@gyu.edu.cn
Guiyang University

Research Article

Keywords: WPU, Phytic acid, Chitosan, Boron nitride, DiDOPO

Posted Date: June 9th, 2026

DOI: https://doi.org/10.21203/rs.3.rs-9885038/v1

License: This work is licensed under a Creative Commons Attribution 4.0 International License.
Read Full License

Additional Declarations: No competing interests reported.

Version of Record: A version of this preprint was published at Journal of Inorganic and Organometallic Polymers and Materials on July 10th, 2026. See the published version at https://doi.org/10.1007/s10904-026-04447-x.

Construction of Waterborne Polyurethane Composites via Phytate-Chitosan-Modied Boron Nitride and DOPO Derivative Synergy: A route to flame retardancy and multifunctional performance

Yanling Yue[1], Bingyue Huang[1], Deyu Liu[1], Shaoyuan Wu[1], Jinghan Hu[1], Shiyi Ming[1], Xingyu Guan[1],Yi Zhang[1]*, Kui Wang[1], Weijiang Huang[1], Wei Yan[1]*

1. School of Materials Science and Engineering, Guiyang University, Guiyang 550005, P.R. China

Abstract: Hexagonal boron nitride (h-BN) is inherently hydrophobic and lacks active functional groups on its surface. In this study, we modified h-BN with phytic acid and chitosan to create BN@PA-CS particles. These particles integrated into an aqueous polyurethane (WPU) matrix, along with the DiDOPO flame retardant, to form the WPU/BN@PA-CS/DiDOPO nanocomposite. We investigated the composite's flame retardancy, thermal stability, rheological properties, and mechanical properties. The results demonstrated that BN@PA-CS and DiDOPO exhibit a significant synergistic effect in both gas and condensed phases for flame retardancy. The optimal formulation, WPU/BN@PA-CS2/DiDOPO7, achieved a UL-94 V-0 rating and increased the limit oxygen index (LOI) to 24.2%. Additionally, the peak heat release rate (pHRR) and total heat release (THR) decreased by 49.3% and 66.1%, respectively, compared to pure WPU. Rheological and mechanical tests indicated that this formulation achieved an ideal balance of stiffness, toughness, and flowability. Therefore, the DiDOPO/BN@PA-CS composite strategy provides both theoretical

and experimental support for developing high-performance flame-retardant polyurethane composites, optimizing synergistic effects at specific ratios to enhance flame re.tardancy and mechanical properties.

Keywords: WPU, Phytic acid, Chitosan, Boron nitride, DiDOPO

1. Introduction

Waterborne polyurethane (WPU), which employs water as the dispersion medium, offers several advantages, including environmental friendliness, safety, high adjustability, excellent mechanical properties, and ease of processing[1].These characteristics contribute to its widespread application in coatings, adhesives, textile coatings, and flexible composite materials. However, pure WPU exhibits poor flame retardancy, rapid heat release during combustion, and a tendency to melt and drip, which pose significant fire hazards and limit its use in high-safety environments. Halogen-free, highly synergistic composite flame retardant systems have emerged as the primary method for modifying WPU. Synergistic strategies that incorporate phosphorus-based and nitrogen-based compounds, along with inorganic nanofillers, effectively utilize the carbon formation benefits of both the gas phase and condensed phase, thereby enhancing the overall flame retardant performance of the material[5].

Hexagonal boron nitride (h-BN) exhibits high thermal conductivity, chemical stability, and layered barrier properties. However, its hydrophobic surface, limited active sites, and poor compatibility with polymer matrices necessitate interface improvement through hydroxylation or grafting techniques[15]. Phytic acid (PA), rich in phosphate groups, forms stable bonds with hydroxylated BN and catalyzes carbon

formation during combustion. Chitosan (CS), a natural nitrogen-containing polysaccharide, collaborates with PA to establish a phosphorus-nitrogen synergistic system that promotes the formation of a dense expanded carbon layer[22].The combined coating of BN with these components enhances filler dispersion and improves flame-retardant efficiency in the condensed phase[28]. DiDOPO, a representative phosphorus-based flame retardant, releases free radicals such as PO and PO_2 in the gas phase, which scavenge highly reactive species like H and OH during combustion, thereby inhibiting chain reactions. The formulation of DiDOPO with BN@PA-CS achieves a triple synergistic effect: gas-phase flame retardancy, condensed-phase catalytic carbon formation, and boron nitride barrier shielding, enhancing flame resistance while maintaining the material's mechanical properties[34].

Systematic research on the synergistic modification of aqueous polyurethane using BN@PA-CS and DiDOPO remains limited. The effects of filler ratios on flame retardancy, thermal stability, rheological properties, and mechanical performance have not been thoroughly investigated, and the underlying synergistic mechanism requires further elucidation[37].To address this gap, this study subjected h-BN to hydroxylation to prepare a BN@PA-CS composite filler with a PA-CS bilayer coating[41]. This filler was blended with DiDOPO to synthesize WPU-based nanocomposites. Comprehensive characterization techniques examined the structural evolution of the composites, revealing how filler ratios regulate flame retardancy, thermal stability, rheological behavior, and mechanical properties. The study elucidates the gas-phase-condensed-phase synergistic flame retardation mechanism

and identifies the optimal formulation. This work provides an experimental foundation and theoretical framework for developing aqueous polyurethane composites with enhanced flame retardancy and mechanical balance.

2. Experimental

2.1 Materials

Water-based polyurethane (WPU), hexagonal BN, PA (70% in H_2O), and CS (deacetylation: >95%, M_η: 55×10^4) were obtained from Aladdin Regents Co., Ltd., Shanghai, China. Concentrated HNO_3 (AR), glacial acetic acid (CH_3COOH ⩾ 99.8%) were purchased from Sinopharm Chemical Reagent Co., Ltd. Deionized water was prepared in our laboratory. All chemicals were used as received without further purification.DIDOPO (prepared in the laboratory),as detailed in Supporting Information Fig.S1.

2.2 Hydroxylation functionalization of boron nitride surface

Hexagonal boron nitride (h-BN) is typically hydrophobic and lacks active functional groups on its surface, limiting its compatibility with polar systems and reducing modification efficiency. In this study, we performed surface hydroxylation of h-BN using the nitric acid oxidation method[43].In a typical procedure, 2.0 g of h-BN powder was added to a three-necked flask containing 100 mL of nitric acid (65%–68%). The mixture was mechanically stirred at 400 r/min and heated in an oil bath at 80 ℃ for 6 h, during which the oxidative etching of nitric acid cleaved B-N bonds on the h-BN surface and introduced hydroxyl (-OH) groups. After the reaction, the

system was allowed to cool naturally to room temperature, and the solid product was collected by vacuum filtration. The filter cake was repeatedly washed with deionized water until the pH of the washings reached 7.0. The resulting hydroxylated boron nitride was dried in a vacuum oven at 60 ℃ for 12 h, yielding a white powder (designated as BN) with a hydroxyl-rich surface that provides reactive sites for subsequent coupling modification and composite preparation.

2.3 Preparation of BN@PA-CS

2.3.1 Preparation of Phytic Acid-Modified Boron Nitride (BN@PA)

Weigh 1.0 g of boron nitride (BN) powder and place it in a beaker with 200 mL of deionized water. Use ultrasonic dispersion for 20 minutes to achieve a uniform suspension of BN powder. Gradually add a 70% phytic acid (PA) aqueous solution to the dispersion. Set the stirring rate to 200 rpm and place the system in a constant temperature water bath at 50℃for 3 hours. The surface modification occurs through the interaction between phosphate groups in phytic acid and hydroxyl groups on the boron nitride surface. After the reaction, transfer the mixture to a high-speed refrigerated centrifuge and centrifuge at 10000 r/min for 8 minutes to separate the precipitate. Repeat the centrifugation process three times to remove unreacted phytic acid, resulting in the phytic acid-modified boron nitride (BN@PA) intermediate[44].

2.3.2 Preparation of Chitosan Acetic Acid Water Solution and Chitosan (CS)

Dispersion: Begin by weighing 0.5 g of chitosan powder and adding it to a three-necked flask with 50 mL of a 22% (w/v) acetic acid aqueous solution. Stir the mixture at 400 rpm using a mechanical agitator. Keep the flask in a water bath at 45°

C for 2 hours until the chitosan fully dissolves, resulting in a homogeneous, transparent solution. Set this solution aside for later use.

2.3.3 Preparation and Purification of BN@PA-CS Composite

Material: Redisperse the prepared BN@PA intermediate in 200 mL of deionized water and ultrasonically disperse it for 5–10 minutes to achieve uniformity. Gradually add this dispersion to the 50 mL chitosan-acetic acid solution while stirring at 400 rpm. Incubate the mixture at 50℃in a water bath for 2 hours. During this process, ionic or hydrogen bonds form between the amino groups of chitosan and the phosphate groups of phytic acid, creating the BN@PA-CS composite structure[45]. Once the reaction concludes, transfer the mixture to a high-speed centrifuge and centrifuge at 10000 r/min for 8 minutes. Repeat this process three times to eliminate unreacted chitosan and impurities. Collect the sediment and dry it in a vacuum oven at 60℃ for 12 hours, yielding the BN@PA-CS composite functional material.

2.4 Preparation of WPU/BN@PA-CS/DiDOPO Nanocomposites

A predetermined mass fraction of BN@PA-CS composite functional powder was weighed and added to an aqueous polyurethane (WPU) matrix. The mixture was subjected to a synergistic “ultrasonic dispersion-mechanical stirring”treatment for 30 minutes to achieve uniform dispersion of BN@PA-CS in the WPU and to prevent agglomeration[46]**Error! Reference source not found.**.Subsequently, under continuous stirring at the same speed, the preset proportion of DiDOPO flame retardant powder was slowly introduced into the dispersion. Stirring continued for 30 minutes to ensure thorough mixing of DiDOPO with the BN@PA-CS/WPU system. Through interactions

between DiDOPO and the surface functional groups of BN@PA-CS, together with physical dispersion effects, a synergistic functional system was formed. After mixing, the composite was vacuum-degassed for 10-15 minutes (vacuum pressure $\leqslant -0.09$ MPa) to remove residual bubbles. The material was then slowly poured into pre-dried custom molds and allowed to cure naturally in a room-temperature ventilated environment (curing time adjusted according to material thickness, typically 72-125 hours) to ensure complete solvent evaporation,yielding a structurally homogeneous WPU/BN@PA-CS/DiDOPO nanocomposite.

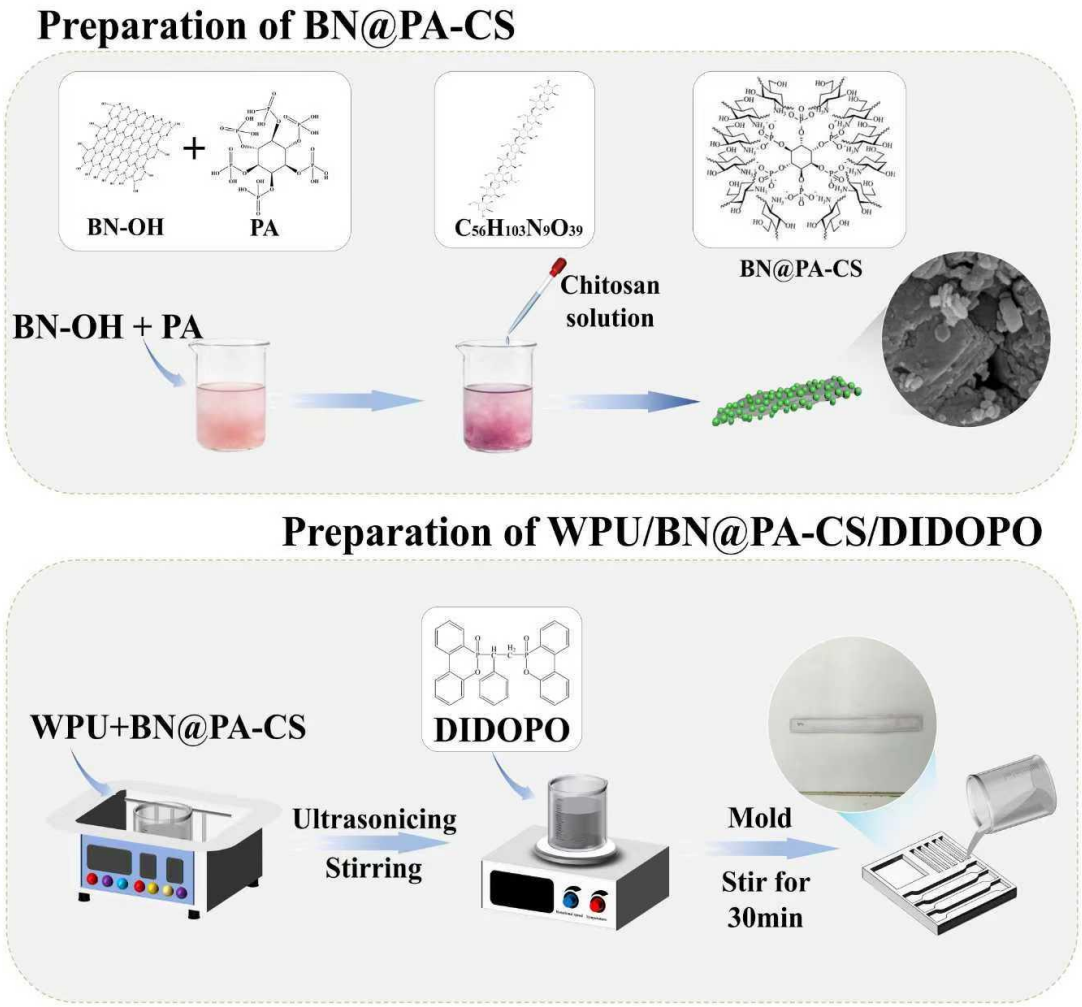


Figure 1. Schematic diagram of BN@PA-CS and WPU/BN@PA-CS/DIDOPO preparation process

2.5 Physical Property Characteristics

X-ray powder diffractometry (XRD,D/MAX2500,Rigaku Corporation,Tokyo,Japan) measurements were conducted using Cu K α radiation (λ =0.15418 nm)over 10-80° at a scan rate of 20° /min to investigate the structure of BN and BN@PA-CS.

To observe the morphologies and compositions of the BN@PA-CS,WPU/BN@PA-CS,and char residues, field-emission scanning electron microscopy (SEM,FEI Quanta 250FEG,FEI Inc.,Valley City,ND,USA;recorded under high vacuum at a voltage of 20 kV) and transmission electron microscopy (TEM, FEI Tecnai G2 20, FEI Inc.,Valley City, ND, USA)were performed.

Fourier-transform infrared (FTIR, Nicolet IS50, Thermo Fisher Scientific Inc.,Waltham, MA, USA)spectroscopy was conducted from 400 to 4000 cm^{-1} at a resolution of 4 cm^{-1},with 32 scans per spectrum,to characterize the structures of BN and BN@PA-CS.

Thermogravimetric analysis (TGA,TG 219 F3,Netzsch Instruments Co.Ltd.,Selb, Germany)was conducted at a constant scan rate of 10 ℃/min under nitrogen at temperatures of 50-800 ℃ to obtain the TGA and differential thermogravimetry (DTG)thermograms.Each sample grade was subjected to three parallel measurements.

An electromechanical tensile tester (Model 5900,Instron Corporation,Norwood,MA, USA)was employed to study the tensile performance of the PVDF with a constant rate of 50 mm/min;the length,width,and thickness of the

samples were 33 mm,6 mm,and 50-80 μm, respectively, and the thickness was measured using a thickness gauge.

The samples were analyzed using energy-dispersive X-ray spectroscopy (EDS,INCA Energy 350,Oxford Instruments,Abingdon,UK) at 20 kV.

The gases released during TGA were investigated using a Nicolet iS50 FTIR spectrometer.TGA-FTIR analysis was conducted using TGA coupled with FTIR spectroscopy. The FTIR spectrum of each sample was collected over 16 scans in the wavenumber range 500-4000 cm^{-1} .

Microscale combustion calorimetry (DEATAK MCC-3, Fire Testing Technology Ltd., East Grinstead,UK)was conducted at temperatures ranging from room temperature to 900 ℃ at a heating rate of 1℃/s to evaluate the flammability of the WPU composite films.

Laser Raman spectroscopy measurements were performed at room temperature using a Renishaw RM2000 Raman apparatus.Samples were excited with a 514 nm laser,and spectra were recorded over a wavelength range of 200-4000 cm^{-1}.

3.Results and discussion

3.1 Structure and morphology of BN@PA-CS

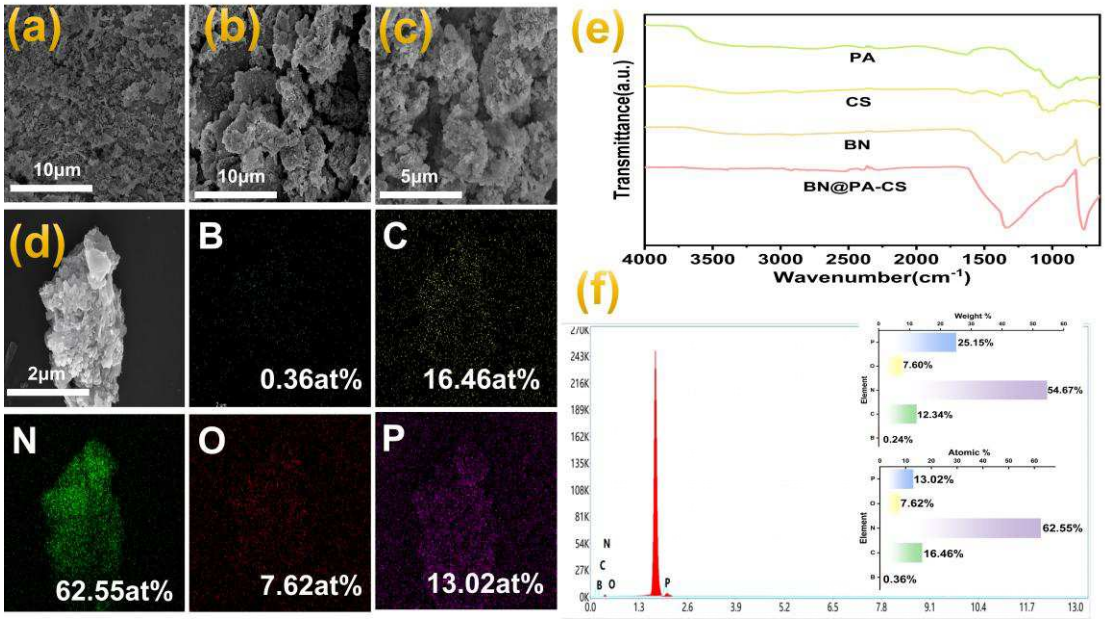


Figure 2.（a）Hydroxylated boron nitride SEM image，（b）（c）BN@PA-CS SEM,（d）BN@PA-CS Mapping,（e）Fourier transform infrared spectrogram，（f）BN@PA-CS spectral analysis

Combining thermogravimetric analysis of the supports (Figure S2) with multidimensional characterization by scanning electron microscopy, elemental surface mapping, and infrared spectroscopy confirms that phytic acid-chitosan composite layers were successfully deposited on hydroxylated boron nitride (BN) sheets treated with concentrated nitric acid, producing structurally stable BN@PA-CS composite fillers. The thermogravimetric curve (Figure 2) shows that pure hydroxylated BN retained nearly 100% of its mass between 25 and 700℃, reflecting the intrinsic thermal stability of the inorganic material. By contrast, pure PA-CS displayed the typical thermal decomposition of organic components with substantial weight loss at moderate to high temperatures. The thermal behavior of BN@PA-CS fell between these two extremes, showing weight-loss features corresponding to the main decomposition range of PA-CS and illustrating the change in thermal stability after combining the inorganic sheets with the organic coating.These observations indicate

successful incorporation of PA-CS onto BN sheet surfaces. Microscopic morphology analysis shows that hydroxylated BN (Figure 2(a)) has smooth, flat surfaces, whereas BN@PA-CS (Figure 2(b,c)) exhibits markedly roughened surfaces with a continuous, uniform organic coating consistent with the expected surface loading. Elemental mapping and energy-dispersive spectroscopy (EDS) (Figure 2(d) – (f)) detect both characteristic BN elements (B, N) and PA-CS-specific elements (C, O, P) in BN@PA-CS; all elements are uniformly distributed across BN sheet surfaces without evident segregation or phase separation, further supporting homogeneous PA-CS loading. Infrared spectroscopy shows that BN@PA-CS retained the characteristic B-N absorption peaks of BN, the phosphorus – oxygen bond peaks of PA, and the amide bond peaks of CS. Notably, pronounced peak broadening and shifts appear in the hydroxyl region, indicating hydrogen-bonding interactions between hydroxyl groups introduced by acid treatment and PA-CS rather than simple physical mixing. Taken together, the characterization data consistently demonstrate that PA-CS was successfully and uniformly loaded onto the hydroxylated BN sheet surface and that the BN@PA-CS composite filler was prepared.

3.2 Combustion Behavior of WPU and WPU/BN@PA-CS/DiDOPO

Figure S3 presents vertical combustion test images for each sample, and Table 1 lists the corresponding UL-94 ratings and limiting oxygen index (LOI) values. A comprehensive analysis showed the following: WPU/BN@PA-CS2/DiDOPO7 produced no melt dripping during either 10-second ignition test and exhibited the fastest self-extinguishing behavior. Upon initial ignition it formed a dense protective

char layer that prevented reignition in the second test; flames were confined to roughly one-third of the sample area, and the sample attained a UL-94 V-0 rating the highest level in this series. WPU/BN@PA-CS7/DiDOPO2 behaved similarly, showing no dripping and rapid self-extinguishing. Although it did not reignite after the second ignition, flame spread covered about half of the sample area and its char layer provided slightly less effective protection than that of WPU/BN@PA-CS2/DiDOPO7, yet it still met UL-94 V-0 requirements.Both WPU/DiDOPO9 and WPU/BN@PA-CS1/DiDOPO8 showed no dripping and met the UL-94 V-1 self-extinguishing criteria; no reignition occurred after the second ignition, yielding an overall V-1 rating. Their flame-retardant performance exceeded that of pure WPU but did not reach the V-0 level. By contrast, WPU/BN@PA-CS8/DiDOPO1, WPU/BN@PA-CS9, and pure WPU exhibited poorer flame retardancy. The first two samples dripped molten material during both ignition attempts and ignited the underlying degreased cotton. Although pure WPU self-extinguished within 30 s without producing dripping ignition, these three samples attained only a UL-94 V-2 rating. Limiting oxygen index (LOI) measurements showed pure WPU at 18.2%. Incorporation of the BN@PA-CS/DiDOPO composite system raised the LOI to 24.2% for WPU/BN@PA-CS2/DiDOPO7, but further increasing BN@PA-CS content caused the LOI to decline to 19.8% for WPU/BN@PA-CS9.This trend demonstrates a pronounced synergistic flame-retardant effect between BN@PA-CS and DiDOPO, producing maximal flame resistance at particular ratios. Excessive BN@PA-CS disrupts this balance and

reduces flame retardancy, indicating an optimal formulation ratio for the composite system. Overall, the WPU/BN@PA-CS2/DiDOPO7 blend showed superior combustion behavior, self-extinguishing rate, char-layer protection efficiency, and LOI values, making it the most flame-retardant formulation in the series. These findings confirm a component-dependent relationship in the BN@PA-CS/DiDOPO system: moderate BN@PA-CS addition enhanced flame-retardant efficacy, whereas excessive amounts degraded performance.

Table 1.UL-94 test results and limited oxygen index (LOI) of WPU composites

Sample	UL-94			LOI
	Does it drip	Should it be lit	Level	(%)
WPU	Yes	No	V-2	18.2
WPU/DIDOPO9	No	No	V-1	21.9
WPU/BN@PA-CS1/DIDOPO8	No	No	V-1	23.1
WPU/BN@PA-CS2/DIDOPO7	No	No	V-0	24.2
WPU/BN@PA-CS7/DIDOPO2	No	No	V-0	21.3
WPU/BN@PA-CS8/DIDOPO1	Yes	Yes	V-2	20.6
WPU/BN@PA-CS9	Yes	Yes	V-2	19.8

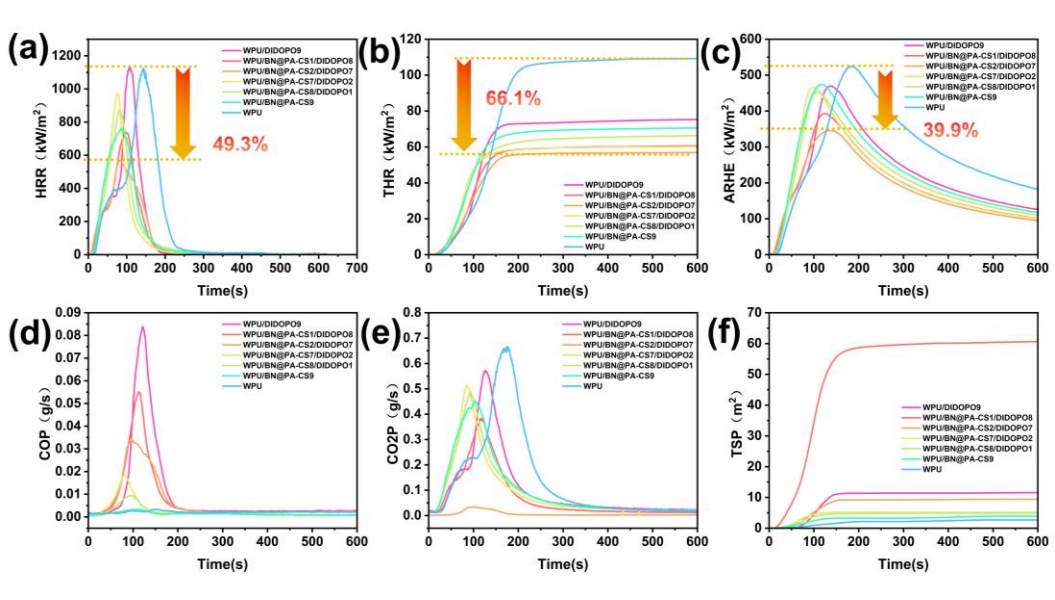


Figure 3. (a) HRR, (b) THR, (c) ARHE, (d) Carbon monoxide emission,(e)carbondioxide production and (f)TSP curves of the WPU/BN@PA-CS/DIDOPO

Table 2. Data obtained from cone calorimeter tests (CCTs) of different samples.

Sample	HRR (kw/m2)	THR (MJ/m2)	ARHE (kw/m2)	CO (g/s)	CO2 (g/s)	TSP (m2)	av-EHC (MJ kg −1)	TML (wt%)
WPU	1125.2	60.1	419.7	0.0032	0.48	2.68	25.27	100
WPU/DIDOPO 9	1132.4	38.3	355.3	0.0026	0.67	5.54	24.55	99.9
WPU/BN@PA-CS1/DIDOPO8	742.0	32.2	331.0	0.0551	0.44	5.42	23.90	98.4
WPU/BN@PA-CS2/DIDOPO7	570.7	20.4	251.5	0.0343	0.34	3.01	21.16	96.1
WPU/BN@PA-CS7/DIDOPO2	973.5	29.2	377.6	0.0008	0.55	3.26	27.82	87.9
WPU/BN@PA-CS8/DIDOPO1	870.3	29.8	362.6	0.0087	0.49	2.67	26.18	85.6
WPU/BN@PA-CS9	760.8	34.7	403.5	0.0007	0.42	1.84	24.69	79.4

(1) Flame inhibition effect:

$$Flame\ inhibition\ effect = 1 - \frac{EHC_{FR-WPU}}{EHC_{WPU}}$$

(2) Barrier and protective effect:

$$Barrier\ and\ protective\ effect = 1 - \frac{\left(\frac{pHRR_{FR-WPU}}{pHRR_{WPU}}\right)}{\left(\frac{THR_{FR-WPU}}{THR_{WPU}}\right)}$$

(3)Charring effect:

$$Charring\ effect = 1 - \frac{TML_{FR-WPU}}{TML_{WPU}} \quad (47)$$

Table 3. Quantitative assessment of the three flame-retardant effects

Sample	Flame-inhibition effect (%)	Barrier and protective effect (%)	Charring effect (%)
WPU	0	0	0
WPU/DIDOPO9	2.85	-65.0	0.1
WPU/BN@PA-CS1/DIDOPO8	5.42	-23.3	1.6
WPU/BN@PA-CS2/DIDOPO7	16.27	-49.1	3.9
WPU/BN@PA-CS9	2.29	-25.0	20.6

Pure WPU exhibitsdisplays typical flammable-polymer behavior: athe peak heat release rate (pHRR) reached 1125.2 kW/m^2, total heat release (THR) was 60.1 MJ/m^2, average effective combustion heat (av-EHC) was 25.27 MJ/kg, and total mass loss (TML) reached 100 wt%. Combustion was intense, with concentrated heat release and minimal char residue. Fire-spread risk was relatively high, withas total smoke production (TSP) atmeasured 2.68 m^2, while overall smoke emission volume remained at the baseline.The flame-retardant data for all composites are summarized in Tables 2 and 3, and the various combustion curves are shown in Figure 3.

Adding DiDOPO to the WPU (sample DIDOPO9) reduced the total heat release (THR) to 38.3 MJ/m^2 (a 36.3% decrease) and the average energy consumption per

unit mass (av-EHC) to 24.55 MJ/kg, indicating a gas-phase flame-retardant effect (flame suppression effect of 2.85%). However, the peak heat release rate (pHRR) rose to 1132.4 kW/m², slightly exceeding that of neat WPU, indicating that DiDOPO alone did not effectively suppress the combustion rate. Instead, it accelerated flame propagation and substantially increased smoke production, revealing clear deficiencies in overall flame-retardant performance.

Among the composites, WPU/BN@PA-CS2/DIDOPO7 exhibited the best overall flame-retardant performance. The pHRR decreased to 570.7 kW/m² (a 49.3% reduction versus pure WPU and a 49.6% reduction versus WPU/DIDOPO9), THR decreased to 20.4 MJ/m² (a 66.1% reduction versus pure WPU and a 46.7% reduction versus WPU/DIDOPO9), and av-EHC decreased to 21.16 MJ/kg (a 16.2% reduction versus pure WPU and a 13.8% reduction versus WPU/DIDOPO9). All of these values were lower than those of pure WPU and WPU/DIDOPO9, effectively delaying flame propagation. TSP increased to 3.01 m², approaching the level of pure WPU and thereby avoiding the smoke-emission surge seen with single-DiDOPO modification.

From the standpoint of flame-retardant mechanisms, the sample was primarily governed by DiDOPO-mediated gas-phase flame suppression (16.27%), with supplementary char-promoting effects catalyzed by BN@PA-CS (3.9%). This synergy produced a substantial reduction in combustion heat release and thermal release rates: the average effective heat of combustion (av-EHC) decreased by 16.2% relative to pure WPU, while the peak heat release rate (pHRR) and total heat release

(THR) declined by 49.3% and 66.1%, respectively. These results underscore the beneficial role of gas-phase-condensed-phase synergistic flame retardancy. In particular, DiDOPO decomposition in the gas phase released PO• radicals that quenched combustion-active species such as H• and OH•, substantially lowering the combustion heat released per unit mass of volatiles[48].

In the condensed phase, BN@PA-CS catalyzes early char formation in WPU, which reduces emission of combustible volatiles and creates physical barriers that further suppress peak heat release rate and total heat release[49]. By contrast, WPU modified only with DiDOPO (WPU/DiDOPO9) exhibited a slightly higher pHRR than neat WPU, indicating that a single flame retardant lacking char-promoting ability cannot effectively control combustion rates. Samples with high BN@PA-CS loading (e.g., WPU/BN@PA-CS9) reached a 20.6% char yield but produced less pHRR suppression than formulations at the optimal ratio, reflecting a reduced gas-phase flame-retardant contribution and a strong dependence on the BN@PA-CS/DiDOPO ratio.

Notably, all modified samples showed negative barrier and protective effects, indicating that the carbon layer’s physical barrier was insufficient, likely because of poor interfacial compatibility between BN@PA-CS and the WPU matrix. Overall, WPU/BN@PA-CS2/DIDOPO7 achieved the best balance among gas-phase flame retardancy, condensed-phase carbon formation, and flue gas release through precise formulation ratios, making it the most promising flame-retardant formulation in this system.

3.3 Gas-phase flame retardant

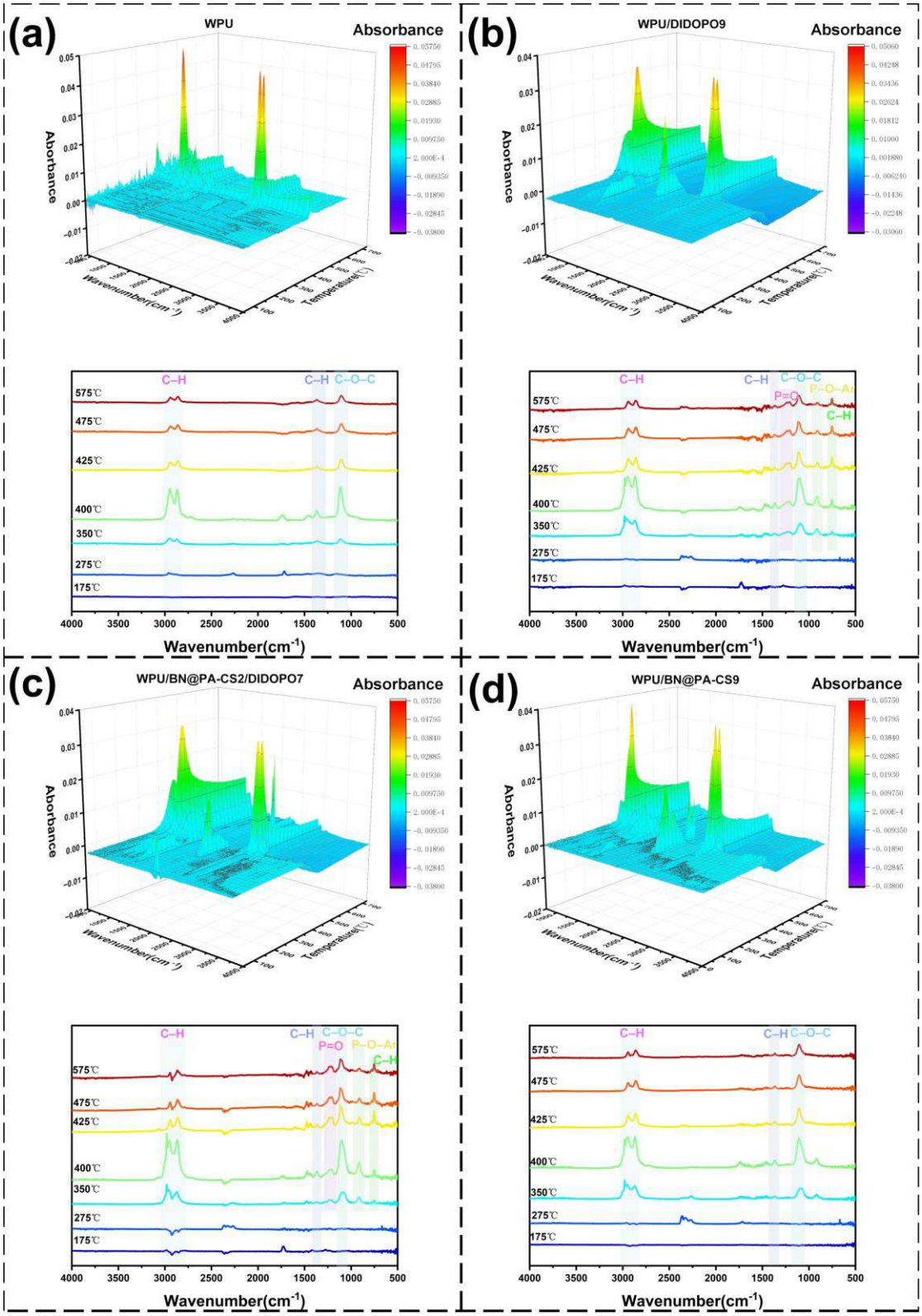


Figure 4 . Three-dimensional TG-IR spectra of WPU (a) ; three-dimensional TG-IR spectra of WPU/DIDOPO9 (b) ; three-dimensional TG-IR spectra of WPU/BN@PA-CS2/DIDOPO7 (c); three-dimensional TG-IR spectra of WPU/BN@PA-CS9 (d);

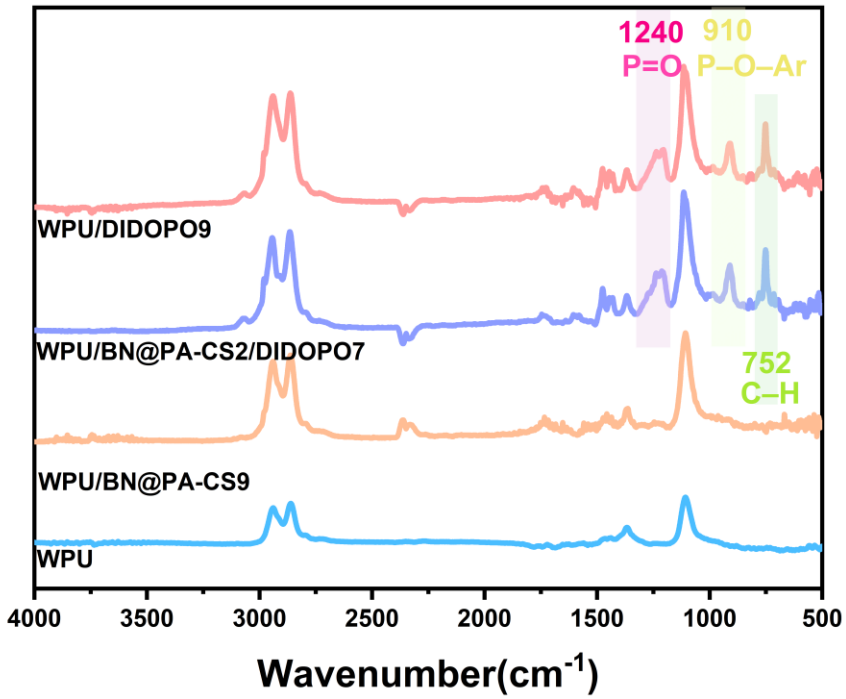


Figure 5 .the release curve at the maximum thermal decomposition temperature

Thermogravimetry-Fourier transform infrared spectroscopy (TG-FTIR,as shown in Figure 4) is a standard technique for analyzing evolved gases, enabling real-time monitoring of volatile gas-phase products and their release profiles during thermal decomposition and providing critical spectroscopic evidence for elucidating gas-phase flame-retardant mechanisms[50]. In this study, TG-FTIR was used to analyze gas-phase behavior during the thermal decomposition of neat WPU and of flame-retardant-modified WPU samples, with emphasis on the interaction mechanisms between DiDOPO-based gas-phase flame retardants and BN@PA-CS carbonization agents.

The gas-phase products from thermal decomposition of neat WPU are released mainly between 275 and 400 °C, with the characteristic peak intensity occurring at

400 °C and declining gradually after 425 °C; faint signals persist at 575 °C.The release curves of all composites at the maximum thermal decomposition temperature are shown in Figure 5. In the ~1100–1250 cm^{-1} region, C–O–C stretching vibration peaks arise from cleavage of ester/ether bonds in the polyurethane rigid segments, producing small ether- and alcohol-derived molecules. At ~1368 cm^{-1}, aliphatic C–H symmetric bending vibrations form a continuous signal series with symmetric and asymmetric C–H stretching vibrations at 2865 cm^{-1} and 2947 cm^{-1}, respectively, collectively indicating cleavage of polyether/polyester backbone chains in the WPU soft segments and release of flammable hydrocarbon fragments such as alkanes and alkenes. Neat WPU showed no characteristic peaks of phosphorus- or nitrogen-containing flame retardants; its combustible volatiles were concentrated at 400 °C and persisted until 575 °C, reflecting the typical thermal decomposition behavior of flammable polyurethanes.

Compared with pure WPU, the WPU/DiDOPO spectrum exhibits distinct features that provide clear spectroscopic evidence of DiDOPO’s gas-phase flame-retardant activity. A P=O stretching vibration appears near 1240 cm^{-1}, attributable to free-radical fragments such as PO and PO_2 released during DiDOPO decomposition. A P-O-Ar stretching vibration appears near 910 cm^{-1}, arising from cleavage of phosphorus-oxygen-aromatic linkages. An aromatic C-H out-of-plane bending vibration is observed near 752 cm^{-1}, consistent with benzene-ring decomposition products. These three characteristic peaks occur only in DiDOPO-containing samples and therefore constitute key evidence for a gas-phase

flame-retardant mechanism. Additionally, the intensity of aliphatic C-H bands decreases relative to pure WPU, and their decay accelerates after peak formation, indicating that DiDOPO incorporation partially inhibits thermal scission in WPU soft segments and reduces emission of combustible hydrocarbons.

The WPU/BN@PA-CS9 sample exhibited no DiDOPO characteristic peaks, indicating a flame-retardant mechanism dominated by condensed-phase carbon formation. The intensities of the aliphatic C-H and C-O-C peaks decreased markedly, their peak temperatures shifted to 400 ℃, and their post-peak decay rates accelerated. These observations indicate that BN@PA-CS catalyzed early carbonization by immobilizing more combustible components within the solid char layer, thereby reducing the supply of gaseous fuel. The absence of phosphorus-containing peaks (P=O and P-O-Ar) in the spectra confirmed that the flame retardancy relied entirely on condensed-phase char formation, with no contribution from gas-phase quenching[46].

The WPU/BN@PA-CS2/DIDOPO7 sample at the optimal ratio exhibited the strongest synergistic effect. The P=O peak intensity near 1240 cm^{-1} was highest, indicating that DiDOPO decomposed most completely and released phosphorus-containing radicals that efficiently quenched the combustion chain reaction. Characteristic peaks of aliphatic C-H and C-O-C bonds had the lowest intensities, with their peak temperatures shifted to higher values and the fastest decay rates. These observations demonstrate that BN@PA-CS and DiDOPO acted synergistically to reduce formation and release of combustible volatiles, retaining

more pyrolysis products in the solid carbon layer rather than allowing them to escape as gases. The main decomposition stage shifted to 400-425 ℃ and proceeded more gradually, indicating that the synergy delayed main-chain cleavage and produced a milder heat-release profile.

In summary, TG-FTIR demonstrated the gas-phase flame-retardant mechanisms and corroborated the combustion-performance tests. Samples that released smaller amounts of gas-phase products and did so for shorter durations exhibited lower heat release rates and reduced total heat release during combustion, resulting in superior flame retardancy. The observed gas-phase product patterns matched the flame-retardancy ranking from cone calorimetry and other combustion tests, thereby validating the combustion-performance conclusions through gas-phase product analysis. Pure WPU continuously released large quantities of combustible volatiles without flame-retardant suppression, whereas WPU/DIDOPO9 achieved gas-phase quenching by releasing phosphorus-containing reactive fragments.Although WPU/BN@PA-CS9 reduces the release of combustible volatiles by promoting char formation, overall emissions remained relatively high because it lacked gas-phase flame-retardant species to quench combustion chain reactions. In this system, WPU/BN@PA-CS2/DIDOPO7 produced a synergistic combination of gas-phase quenching and condensed-phase char formation. This dual mechanism reduced the generation and release of combustible volatiles at the source and enabled efficient quenching of combustion chains by phosphorus-containing free radicals, demonstrating superior control over thermal decomposition behavior[51].

3.4 Solid-phase flame retardant

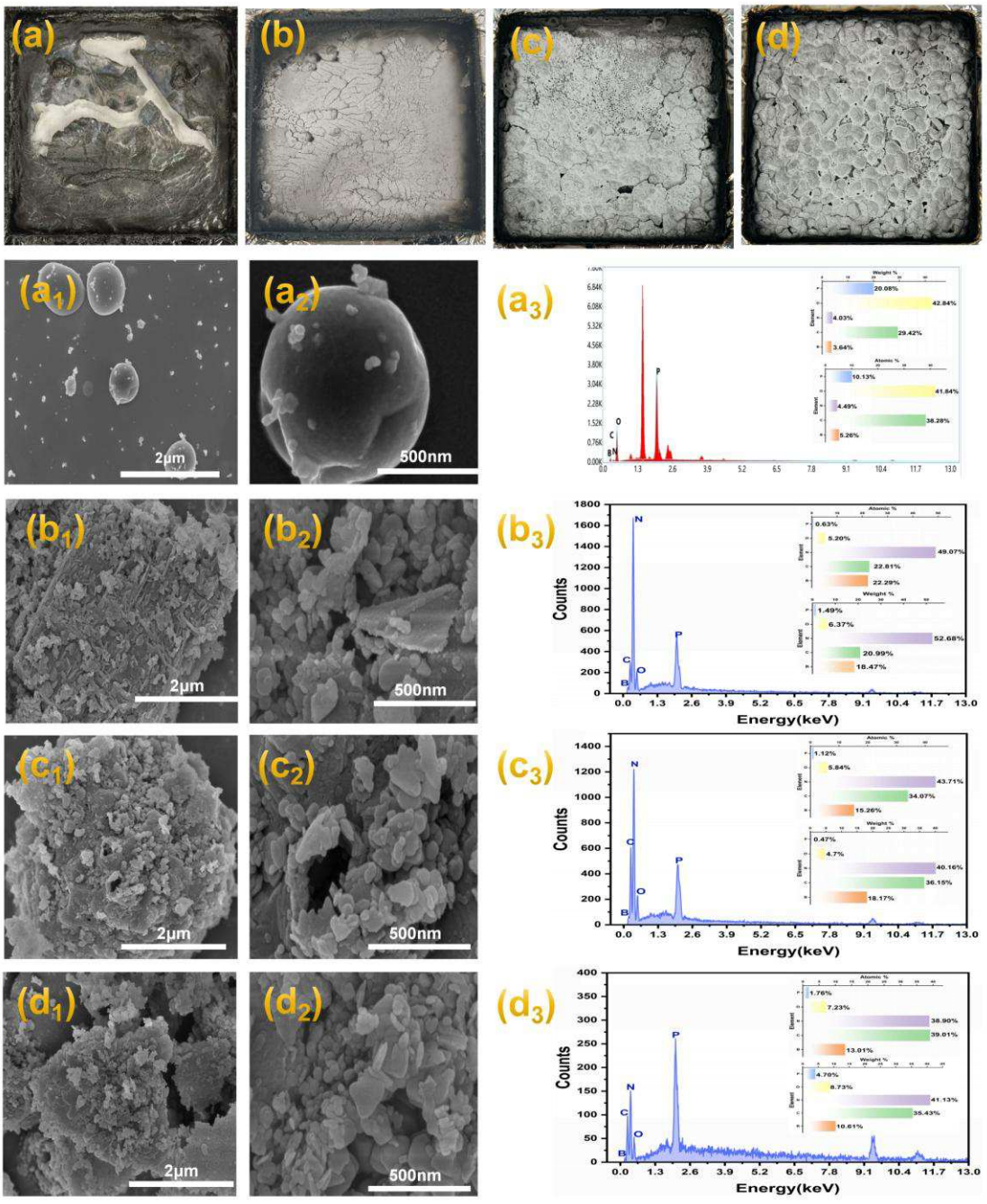


Figure 6. Digital photographs and corresponding SEM images of the char residues after the CCT for (a 、 a_1 and a_2) neat WPU/DIDOPO9, (b 、 $b_1$and b_2) WPU/BN@PA-CS2/DIDOPO7, (c 、 c_1 and c_2) WPU/BN@PA-CS8/DIDOPO1, and (d、d_1 and d_2) WPU/BN@PA-CS9. (a3) EDS data for WPU/DIDOPO9, (b3) EDS data forWPU/BN@PA-CS2/DIDOPO7,(c3) EDS data for WPU/BN@PA-CS8/DIDOPO1，(d3) EDS data for WPU/BN@PA-CS9

Using multi-scale characterization of macroscopic morphology, microscopic

structure, elemental distribution, and the support material’s Raman spectra (Figure S4), we observed substantial differences in solid-phase flame-retardant behavior among the samples. The optimal system, WPU/BN@PA-CS2/DIDOPO7(Figure 6b), exhibited strong synergistic regulatory effects, while other formulations showed clear limitations.

The unmodified sample WPU/DIDOPO9 (Figure 6a) left minimal residual carbon after cone calorimetry, and its char layer exhibited pronounced shrinkage and local collapse, indicating poor structural integrity. At the microscopic level, the residue consisted mainly of dispersed hollow spherical microspheres with numerous cracks and pores that prevented formation of an effective physical barrier. EDS detected only C, N, O, and P and no B signal, with low carbon content and relatively high oxygen content. These findings indicate that DiDOPO suppressed flame propagation primarily by gas-phase quenching and failed to catalyze WPU crosslinking into a stable carbon framework. Consequently, the char remained porous and highly oxidized, contributed negligibly to solid-phase flame retardancy, and accounted for the sample’s poor flame-retardant performance.

The residual char of the optimal system WPU/BN@PA-CS2/DIDOPO7(Figure 6b) exhibited an expanded morphology with intact carbon layers and no significant surface damage. At the microscale, it formed a continuous, dense, closed-pore structure with uniform pore distribution and minimal surface defects, characteristic of a high-quality expanded carbon layer. EDS analysis showed a uniform distribution of flame-retardant elements-nitrogen (N), phosphorus (P), and boron (B)-tightly

integrated with the carbon framework, confirming excellent dispersion of BN@PA-CS2 in the matrix and its synergistic interaction with DIDOPO during combustion. BN@PA-CS2 catalyzed early dehydration and cross-linking of WPU to form a stable carbon skeleton, enhancing solid-phase barrier properties, while DIDOPO released phosphorus-containing radicals that quenched combustion chains and provided gas-phase flame retardancy. Together, these effects produced an optimal balance of carbon yield, expansion degree, microstructural density, and uniformity of flame-retardant element distribution, demonstrating exceptional condensed-phase flame-retardant efficiency.

Sample WPU/BN@PA-CS8/DIDOPO1 (Figure 6c) exhibited greater carbonization capability than the unmodified system, but its carbon-layer integrity and uniformity were slightly worse than those of (Figure 6b). At the microscopic level, the carbon-layer density remained acceptable, yet localized uneven pore structures were observed. EDS analysis indicated enrichment of flame-retardant elements, but their distribution was nonuniform, showing pronounced signal fluctuations in some regions. These observations matched structural defects seen in SEM images and suggested that the flame-retardant component ratio had not achieved optimal synergy, resulting in incomplete utilization of the solid-phase barrier effect.

Sample WPU/BN@PA-CS9 (Figure 6d) produced a higher carbonization yield and, at the macroscopic scale, formed continuous carbon layers because of the increased BN@PA-CS content. However, its microstructure showed notable defects: high-magnification images revealed microcracks and brittle fracture zones within the

carbon layers. Although EDS indicated high concentrations of flame-retardant elements, their localized enrichment generated stress-concentration zones that reduced the mechanical integrity of the carbon layers, diminished structural stability, and yielded worse flame-retardant performance than (Figure 6b). These results indicate that, in this composite flame-retardant system, flame-retardant efficiency does not increase monotonically with BN@PA-CS content; excessive addition disrupts the carbon-layer structure and, paradoxically, weakens the solid-phase flame-retardant performance.

Figure S4 in the supporting material (Raman spectrum) shows that all sample carbon layers exhibit the characteristic peaks of carbon materials. The D-to-G peak intensity ratio serves as a primary indicator of the structural order and density of the carbon layers. A lower ratio indicates more ordered, denser carbon layers, which have yielded improved flame retardancy and barrier performance[52].

The sample with the highest DiDOPO addition ratio exhibited the greatest number of defects in its carbon layer, lower structural order, and a relatively loose morphology, which impaired its flame-retardant protection. After introducing the BN@PA-CS composite, the overall D/G ratio decreased, and the optimal formulation reached the lowest value. This result indicates that the carbon layer in that system achieved the highest degree of graphitization and structural order, producing a more compact, intact layer and thus superior flame-retardant performance.

As the BN@PA-CS content increased further, the carbon-layer ratio slightly rebounded, indicating a reduction in the carbon layer's order and density and an

increase in defects. This degradation produced varying degrees of flame-retardant loss in high-filler samples. The observed trend matches the measured flame-retardancy ratings and the carbon-layer morphologies for each system, showing that microstructural characteristics decisively determine overall flame-retardant performance.

In summary, WPU/BN@PA-CS2/DIDOPO7 (Figure 6b) achieved a synergistic "gas-phase quenching and condensed-phase carbonization" effect through optimized formulation design, producing continuous, dense, and structurally stable expanded carbon layers. This system exhibited the best solid-phase flame-retardant performance in the study. Other formulations either lacked carbonization capability or developed structural defects due to component-ratio imbalances and thus failed to reach ideal flame-retardant performance. These findings provide direct evidence to guide future formulation optimization of composite flame-retardant systems.

3.5 Thermal Stability Analysis

Table 4. TG and DTG data of flame-retardant WPU composites under N_2 atmosphere

Sample	T5% (℃)	Tmax-1 (℃)	Tmax-2 (℃)	Residual mass (%)
WPU	181.0	289.9	417.9	0.2
WPU/DIDOPO9	165.5	264.5	394.5	0.7
WPU/BN@PA-CS1/DIDOPO8	171.3	310.6	399.5	3.7
WPU/BN@PA-CS2/DIDOPO7	230.5	318.8	401.6	5.3
WPU/BN@PA-CS7/DIDOPO2	209.0	270.1	401.9	25.0
WPU/BN@PA-CS8/DIDOPO1	240.5	271.5	403.8	28.4
WPU/BN@PA-CS9	252.0	278.8	403.8	36.2

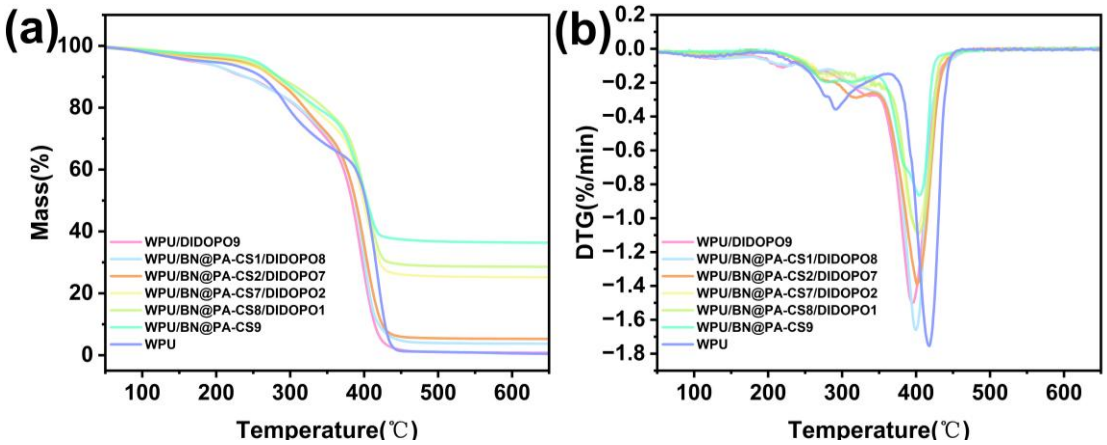


Figure 7. TGA (a) and DTG (b) curves and the division of decomposition stages

The detailed TG/DTG data are shown in Table 4.Combined thermogravimetric (TG) and derivative thermogravimetric (DTG) analyses (Figure 7) show that the BN@PA-CS and DiDOPO composite system substantially enhances the thermal stability and char-forming capacity of WPU while imposing only minor limitations. Pure WPU exhibits poor thermal stability and minimal char formation, with an initial decomposition temperature (T_5%) of 181.0℃. Its two major thermal decomposition peaks occur at 289.9℃and 417.9℃, and the residual carbon content at 800℃is only 0.2%, indicating near-complete decomposition. Introducing the flame-retardant components markedly improved performance: high-temperature residual carbon increased to 36.2% for WPU/BN@PA-CS9 and to 28.4% and 25.0% for WPU/BN@PA-CS8/DIDOPO1 and WPU/BN@PA-CS7/DIDOPO2, respectively. These results indicate that BN@PA-CS and DiDOPO synergistically formed a stable carbon layer that effectively suppressed deep thermal degradation. The first decomposition peak generally shifted to higher temperatures—for example, it

appeared at 318.8° C in WPU/BN@PA-CS2/DIDOPO7—reflecting a substantial improvement in low-temperature thermal stability. Selected optimized formulations showed markedly increased $T_{5\%}$values: WPU/BN@PA-CS2/DIDOPO7, WPU/BN@PA-CS8/DIDOPO1, and WPU/BN@PA-CS9 reached T_5% of 230.5° C, 240.5℃, and 252.0℃, respectively, thereby widening the material's usable temperature range.

The system exhibits minor limitations: the initial decomposition temperatures of some samples decrease slightly—for example, WPU/DIDOPO9 (165.5℃) and WPU/BN@PA-CS1/DIDOPO8 (171.3 ℃) — which is attributed to premature decomposition of DiDOPO or to low concentrations of BN@PA-CS at lower temperatures. The second thermal decomposition peak is generally lower than that of pure WPU (394.5–403.8℃ for modified samples versus 417.9℃ for pure WPU), indicating some loss of structural stability at high temperature. Overall, the BN@PA-CS composite system with DiDOPO significantly enhanced WPU's high-temperature carbonization capacity and low-temperature thermal stability. Despite these minor limitations, its overall thermal stability performance still far exceeded that of pure WPU, providing a reliable basis for flame-retardant material design.

3.6 Flame Retardant Mechanism

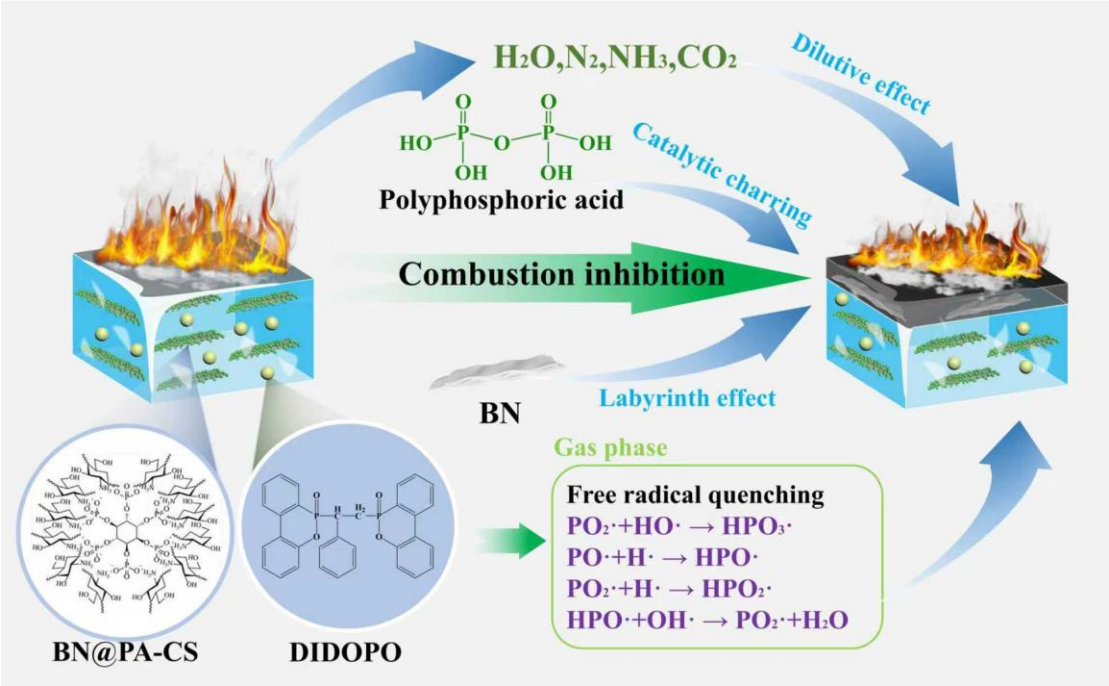


Figure 8. WPU/BN@PA-CS/DIDOPO composite material flame retardant mechanism diagram

As shown in Figure 8,the BN@PA-CS/DIDOPO composite exhibits superior flame retardancy through three synergistic mechanisms. First, in the gas phase, phosphorus-containing radicals released during DIDOPO thermal decomposition scavenge highly reactive combustion radicals. Simultaneously, phytic acid, chitosan, and nonflammable gases produced by DIDOPO pyrolysis (H_2O, N_2, NH_3, CO_2) dilute oxygen and combustible volatiles in the flame zone, disrupting chain reactions[56]. Second, in the condensed phase, a polyphosphate catalytic matrix formed from phytic acid decomposition catalyzed chitosan dehydration and carbonization. Chitosan acted as a nitrogen-rich carbonization framework and, together with phytic acid, formed

P-N synergistic structures that produced continuous, dense phosphorus and nitrogen-rich carbon layers[45].Third, boron nitride provided a barrier effect: two-dimensional BN nanosheets created tortuous physical barriers within the matrix and, together with the carbon layers, formed a compact carbon-ceramic composite barrier. This barrier markedly slowed heat, oxygen, and combustible gas transport, suppressed combustion progression, and substantially improved fire safety performance[58].

3.7 Rheology and Mechanical Analysis

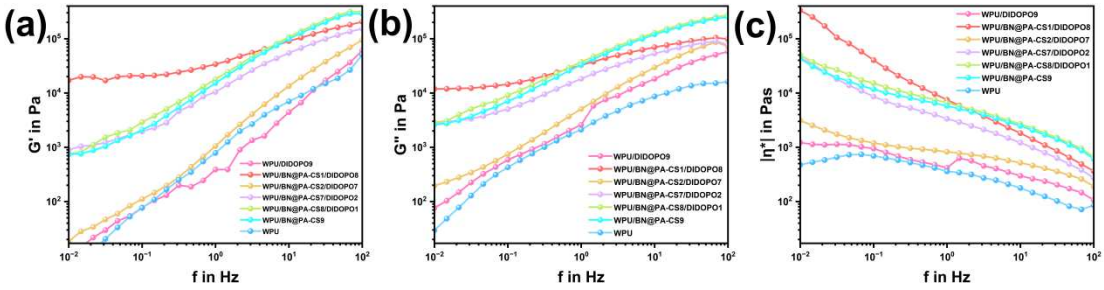


Figure 9. (a–c) Frequency-dependent behavior of the storage modulus, loss modulus, and complex viscosity for WPU and its composite materials.

Dynamic rheological tests showed that incorporating BN@PA-CS and DiDOPO markedly improved the network stability of WPU,as shown in Figure 8. Analysis of the storage modulus (G′,Figure 9a), loss modulus (G″,Figure 9b), and complex viscosity (|η*|,Figure 9c) revealed that all samples displayed typical polymer melt rheological behavior: G′ increased with frequency, while |η*| exhibited shear thinning. The G′ data indicate that all modified samples had greater elastic stiffness than pure WPU.

Specifically, WPU/BN@PA-CS1/DIDOPO8 exhibited relatively high G′ only in

the low-to-mid frequency range rather than across the entire spectrum. The elevated modulus in the mid–low frequency range is more likely attributable to strengthened internal network interactions within the system rather than to filler aggregation. WPU/DIDOPO9 showed consistently lower G′ across the frequency range, remaining below the BN@PA-CS-containing samples from low to high frequencies. WPU/BN@PA-CS2/DIDOPO7 had G′ values higher only than those of pure WPU and WPU/DIDOPO9 and remained overall low; however, this formulation achieved an optimal balance between structural rigidity and chain-segment mobility, yielding superior structural coordination.

The loss modulus indicates that the modified system dissipates more energy overall. The loss modulus of WPU/BN@PA-CS2/DIDOPO7 remains at a moderately low level, while systems with higher BN@PA-CS content exhibit substantially higher loss moduli. However, an excess of rigid components greatly restricts chain-segment mobility, producing a material that is predominantly elastic and brittle. This finding is consistent with the microcracks observed in the carbon-layer scanning electron microscopy images of high-filling samples. Complex viscosity, which reflects melt strength and processing fluidity, shows shear-thinning behavior in all samples.

Pure WPU had the lowest viscosity, weak melt strength, and a tendency to flow and collapse at high temperatures-consistent with thermogravimetric analysis showing extremely low residual carbon content and discontinuous carbon-layer fragmentation after combustion. WPU/DIDOPO9 likewise showed low viscosity among the modified samples, with only marginal improvement from intermolecular chain

interactions and no effective carbon-supporting network, as indicated by its porous carbon-layer structure in scanning electron microscopy. By contrast, WPU/BN@PA-CS2/DIDOPO7 maintained a moderate viscosity that preserved melt integrity during initial combustion without compromising processing fluidity; this balance facilitated the continuous, stable formation of an expanded carbon layer, as corroborated by its more intact carbon-layer morphology in cone calorimetry tests.

In conclusion, the combination of BN@PA-CS and DiDOPO effectively enhanced the rheological and structural stability of WPU. Although the modulus and viscosity of WPU/BN@PA-CS2/DIDOPO7 were not particularly high, its viscoelastic properties showed more rational coordination, yielding a superior overall balance among the formulations. Other systems exhibited problems such as excessive rigidity, insufficient fluidity, or weak structural support. This rheological perspective clarified the intrinsic reasons for variations in flame-retardancy performance across different formulation ratios[53].

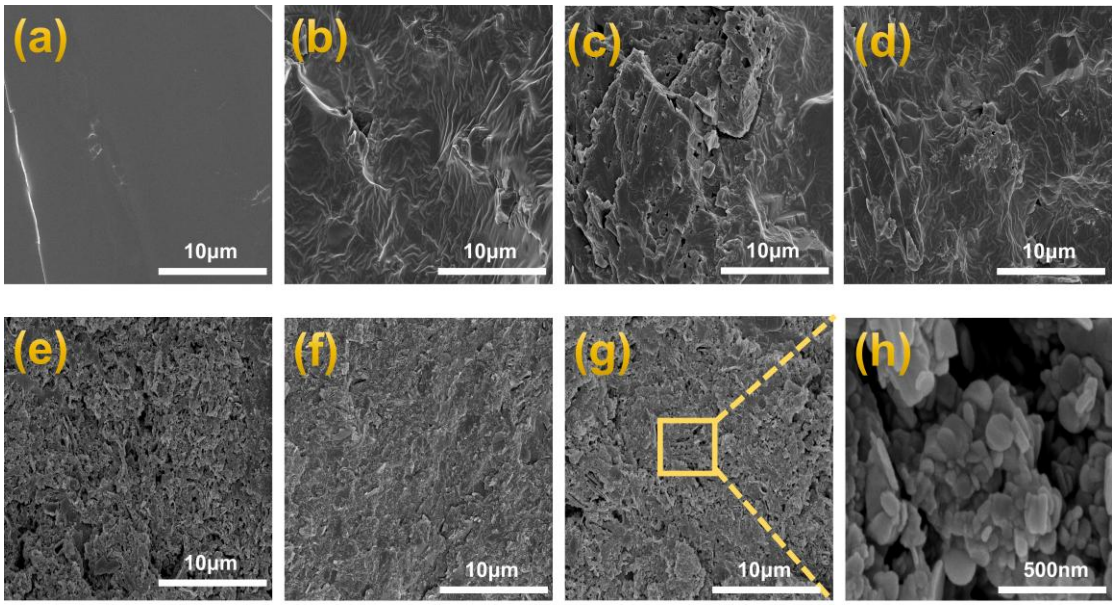


Figure 10. SEM images of the fracture surfaces of (a) wpu,
(b)WPU/DIDOPO9,(c)WPU/BN@PA-CS1/DIDOPO8,
(d)WPU/BN@PA-CS2/DIDOPO7
(e)WPU/BN@PA-CS7/DIDOPO2,(f) WPU/BN@PA-CS8/DIDOPO1
(g)WPU/BN@PA-CS9

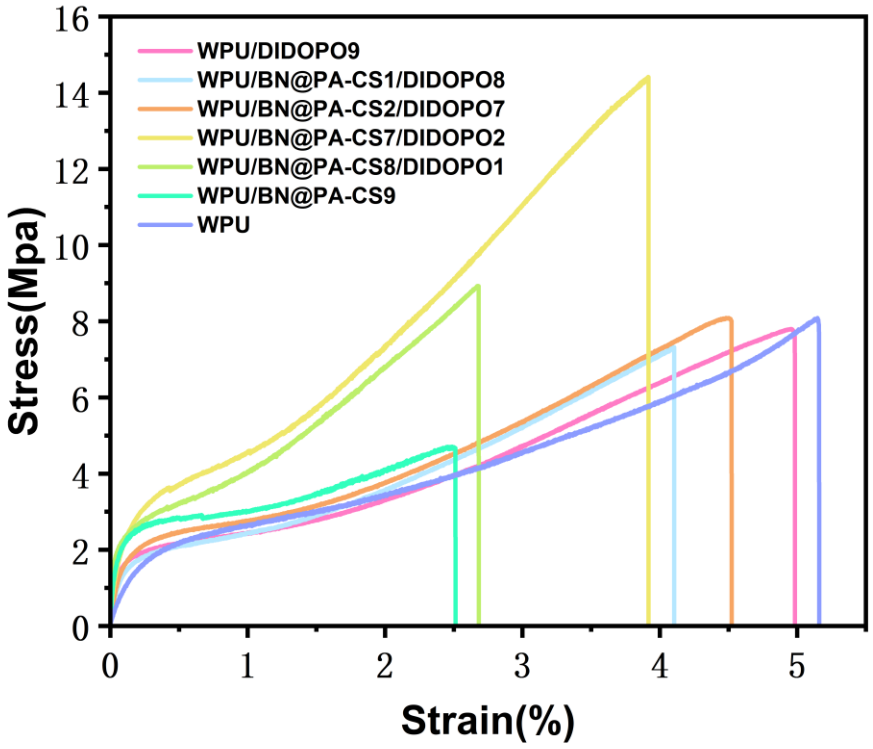


Figure 11. Tensile stress-strain curve for WPU and WPU/BN@PA-CS/DIDOPO

Table 5. Mechanical property data of WPU composite materials

Sample	Tensile strength (MPa)	Elongation at break (%)
WPU	8.08	514.71
WPU/DIDOPO9	7.79	495.10
WPU/BN@PA-CS1/DIDOPO8	7.32	410.39
WPU/BN@PA-CS2/DIDOPO7	8.09	448.48
WPU/BN@PA-CS7/DIDOPO2	9.88	357.65
WPU/BN@PA-CS8/DIDOPO1	8.94	269.73
WPU/BN@PA-CS9	4.70	248.84

The effects of BN@PA-CS and DiDOPO composite modification on WPU mechanical properties depend strongly on composition, and the stress-strain behavior

and tensile data closely match the cross-sectional morphology. The mechanical property data are shown in Table 5.

Pure WPU exhibits the high ductility typical of soft polyurethane, with a tensile strength of 8.08 MPa and a fracture elongation of 514.71%. Its cross section (Figure 10a) is smooth and flat, lacking obvious wrinkles or particles, which is consistent with a ductile fracture produced by full chain slip and orientation during tensile testing. The DiDOPO-modified system (WPU/DiDOPO9) shows a slightly lower tensile strength (7.79 MPa) and fracture elongation (495.10%) than pure WPU; its cross section (Figure 10b) exhibits minor wrinkles and reduced plastic deformation. These observations indicate that DiDOPO molecules modestly interfere with chain entanglement and slip in WPU, producing a small negative effect on mechanical properties.

In the low-ratio BN@PA-CS system, the tensile strength of WPU/BN@PA-CS1/DIDOPO8 decreased further to 7.32 MPa, and the elongation at break fell to 410.39%. The cross section (Figure 10c) showed increased wrinkling and reduced signs of plastic deformation, indicating that BN@PA-CS did not fully realize its reinforcing potential because of insufficient interfacial interactions; molecular chain slip remained partially restricted, causing the strength loss and a slight decrease in toughness. By contrast, WPU/BN@PA-CS2/DIDOPO7 exhibited tensile strength comparable to that of pure WPU (8.09 MPa) and retained a high elongation at break (448.48%). Its cross section (Figure10 d) displayed uniform plastic-deformation wrinkles, reflecting an optimal balance between filler dispersion and interfacial

compatibility. This configuration provided adequate rigidity while preserving chain-segment mobility, yielding coordinated mechanical properties.

The medium-composition BN@PA-CS systems (WPU/BN@PA-CS7/DIDOPO2, WPU/BN@PA-CS8/DIDOPO1) showed an increase in strength accompanied by a decrease in toughness. WPU/BN@PA-CS7/DIDOPO2 reached the highest tensile strength in this study, 9.88 MPa, while its fracture elongation fell to 357.65%. WPU/BN@PA-CS8/DIDOPO1 exhibited a tensile strength of 8.94 MPa and a further reduced fracture elongation of 269.73%. Corresponding cross-sections (Figures 10e, f) revealed greater densification and smaller plastic-deformation zones, indicating that higher BN@PA-CS content enhanced filler-matrix interfacial interactions and more effectively transferred stress to improve strength. However, the resulting restriction of molecular-chain slip substantially reduced toughness, producing a transition to a “strong yet brittle” fracture mode.

The mechanical properties of the high-ratio WPU/BN@PA-CS9 system deteriorated markedly: tensile strength fell to 4.70 MPa and elongation at break decreased to 248.84%. The cross-sectional morphology of WPU/BN@PA-CS9 (Figure 10g) showed a rough surface with pronounced BN@PA-CS particle agglomeration. Figure 10h, a localized magnification of Figure 10g, clearly demonstrated defects and stress-concentration points caused by filler aggregation. Excessive filler disrupted the continuity of the WPU matrix, impeded stress transfer, and produced a typical brittle fracture, causing simultaneous losses in strength and toughness.

In summary, the evolution of mechanical properties in DiDOPO-modified BN@PA-CS composites was closely related to filler dispersion and interfacial interactions. Low-to-moderate ratios (WPU/BN@PA-CS2/DiDOPO7) achieved the best balance between strength and ductility. Medium-to-high ratios increased strength but also increased brittleness. Excessive addition (WPU/BN@PA-CS9) caused an overall deterioration of mechanical properties due to filler agglomeration. This trend corresponded with the morphological transition from ductile to transitional to brittle fracture and supported a mechanistic link between macroscopic mechanical behavior and microscopic fracture processes across the different ratio systems[54].

4. Conclusions

A WPU composite with an integrated flame-retardant system, exhibiting both physical barrier and chemical effects, was successfully fabricated by constructing a core–shell structured BN@PA-CS hybrid and combining it with DiDOPO. The performance of this DiDOPO-BN@PA-CS system was evaluated, revealing that the optimized formulation, WPU/BN@PA-CS2/DiDOPO7, promoted the formation of a continuous, dense protective char layer with a high char yield through condensed-phase catalysis of BN@PA-CS, while excessive BN@PA-CS disrupted the synergistic balance and resulted in a brittle char with pronounced cracks. Notably, pure WPU achieved only a UL-94 V-2 rating and a limiting oxygen index (LOI) of 18.2%, whereas WPU/BN@PA-CS2/DiDOPO7 reached V-0 with an LOI of 24.2%, accompanied by superior self-extinguishing behavior and a markedly reduced peak heat release rate in cone calorimetry. Dynamic rheological and tensile tests further

demonstrated that this composition attained the best balance of rigidity, toughness, and fluidity, retaining high ductility while supporting stable char formation; in contrast, higher BN@PA-CS loading caused filler agglomeration and a simultaneous decline in both mechanical and flame-retardant properties. This enhanced performance is attributed to an efficient triple-synergistic mechanism: BN@PA-CS acts in the condensed phase to catalyze charring and build a physical barrier, whereas DiDOPO quenches free radicals and regulates decomposition pathways in the gas phase. Based on a multidimensional evaluation, WPU/BN@PA-CS2/DiDOPO7 was identified as the optimal formulation that achieves an excellent balance between fire safety and mechanical integrity. The composite system, combining the core–shell structure of BN@PA-CS with DiDOPO, provides innovative design concepts and a practical foundation for developing high-performance flame-retardant waterborne polyurethane materials.

CRediT authorship contribution statement Yanling Yue: Writing-original draft preparation. Bingyue Huang: Writing-review&editing. Deyu Liu**:** Data curation. Shaoyuan Wu**:** Data curation. Jinghan Hu**:** Data curation.Shiyi Ming: Formal analysis. Xingyu Guan:Methodology.Yi Zhang: Methodology, Investigation.Kui Wang: Conceptualization, Weijiang Huang: Software. Wei Yan: Software, Investigation, Funding acquisition.All authors reviewed the manuscript.

Corresponding Author

Yi Zhang School of Materials Science and Engineering, Guiyang University, Guiyang 550005, P.R. China. Email: yikizhang1991@163.com

Wei Yan School of Materials Science and Engineering, Guiyang University, Guiyang 550005, P.R. China.

orcid.org/0009-0007-1305-7478 ; yw2410@gyu.edu.cn

Notes

The authors declare no competing ffnancial interest.

Acknowleggments

This work was nancially supported by the Natural Science Foundatio n of China(52063005), Guizhou Science and Technology Cooperation Project Central-Guided Local Project ([2026]005), Guizhou Provincial Science and Technology Plan Project ([2025]013，[2025]013，［2025]029), Guizhou Science and Technology Cooperation Project Central—Guided Local Project ([2025] 013).

References

1. X. Hu, Y. Zhang, H. Guo, et al., “Multifunctional Flexible WPU Composite Aerogels with Sandwich Structure for Dual-Sided Low-Reflection Electromagnetic Interference Shield ing,” Advanced Functional Materials 36 (2026): 202517665.
2. X. Xu, X. Yang, G. Du, et al., “Improved Interfacial Interaction in PP/Magnesium Hydr oxide Composites via WPU Grafting,” Polymers for Advanced Technologies 37 (2026): e7 0580.
3. B. Ma, W. Jia, Q. Yang, et al., “Enhanced Waterproofing and Adhesion of Emulsified Asphalt via WER/WPU Composite Multi-Component Modification,” Construction and Build ing Materials 506 (2026): 145042..
4. Z. Zhang, R. Mu, H. Zhao, et al., “Thermoplastic and Recyclable EGaIn-SEBS/WPU Fi bers via Wet Spinning with Ultrahigh Stretchability and High Electrical Conductivity,” AC S Applied Polymer Materials 43 (2026): 13977.
5. Y. Ding, L. Sun, G. Liu, et al., “Enhancing the Fire Safety of Waterborne Polyurethane Coatings via Water-Soluble Nitrogen-Phosphorus Flame Retardants,” Colloids and Surfaces A: Physicochemical and Engineering Aspects 740 (2026): 140248.
6. H. Chen, W. Zeng, J. Mei, et al., “Enhancing Flame Retardancy, Mechanical Strength, a

nd Self-Healing Property of Waterborne Polyurethane via Diselenide and Modifying Al/Zn @Phytic Acid," Chemical Engineering Journal 531 (2026): 173962.
7. C. Liu, J. Yang, M. Chen, et al., "Synthesis of DOPO-Containing Melamine Flame Reta rdant and Its Effect on the Flame-Retardant Properties of Waterborne Polyurethane," Journa l of Applied Polymer Science143 (2026): e58046.
8. X. Xu, X. Yang, G. Du, et al., "Improved Interfacial Interaction in PP/Magnesium Hydr oxide Composites via WPU Grafting," Polymers for Advanced Technologies 37 (2026): e7 0580.
9. L. He, Z. Sui, Q. Zhang, et al., "Phytic Acid-Chitosan/Silicone Polyurethane Composite Coating: A Versatile Strategy for Flame-Retardant, Water-Repellent, and Antibacterial Hemp Cellulose Fabrics," International Journal of Biological Macromolecules 361 (2026): 15202 2.
10. N. Xiao, W. Wang, C. Ding, et al., "Castor Oil/DOPO-Based Waterborne Polyurethane with Flame Retardancy-Strength Balance for Microfiber Leather," Chemical Engineering Jo urnal 529 (2026): 173207.
11. J. Zhu, L. Zhang, and C. Li, "Enhanced Flame Retardancy and Mechanical Properties of Waterborne Polyurethane via a DOPO-Based Reactive Flame Retardant," Industrial & E ngineering Chemistry Research 65 (2026): 2769-2779.
12. X. Zhan, J. Chen, Z. Yang, et al., "Fabrication of Multifunctional Waterborne Polyure thane Coatings with Flame Retardancy and Hydrophobicity via Phosphorus-Silicon Synergy and CNC Reinforcement," Progress in Organic Coatings 210 (2026): 109710.
13. D. Hong, Y. Xiang, P. Zhang, et al., "Flame Retardance, Smoke Suppression, Hydroph obicity and Microphase Separation of Waterborne Polyurethane Containing Polyphosphate a nd Silicone Diol," Journal of Applied Polymer Science 143 (2026): e58167.
14. M. Zhang, Z. Sui, L. He, et al., "Synergistic Strategy of Nano-ZnO/DOPO/Fluorinated Silicone in Waterborne Polyurethane Coating for Multifunctional Finishing of Hemp Fabric," Progress in Organic Coatings 216 (2026): 110165.
15. J. Fu, B. Liu, D. Jiang, et al., "Design and Flame-Retardant Synergism of a Green P hosphorus-Containing Heterocyclic Compound in Rigid Polyurethane Foam," Journal of Vin yl and Additive Technology 48 (2026): 70080.
16. K. D. Jayan and K. Deshmukh, "Recent Advances in Nanostructured Boron Nitride Ba sed Flame Retardant Composites: A Comprehensive Review," Sustainable Materials and Te chnologies 47 (2026): e01827.
17. J. Chen, L. Rong, Z. Lu, et al., "Fluorinated Flame Retardant Polyurethane Solid Pol ymer Electrolyte Regulated by Active Surface Defect of Hydroxy-Boron Nitride," Materials Today Chemistry 54 (2026): 103638.
18. D. Shi, Y. Hou, S. Liu, et al., "Flame Retardancy of Boron Nitride-Reinforced Silicone Encapsulants: From Material Design to Performance Reinforcement," Polymer Degradation and Stability 245 (2026): 111920.
19. J. Lin, J. Yu, D. Meng, et al., "A Heat Transfer-Combustion Model for Epoxy Resin/B oron Nitride Nanosheets Composite Materials," Combustion Science and Technology*25 (2 026): 2649461.
20. X. Shi, X. Du, and Y. Han, "Enhanced Flame Retardancy of Polyamide 6 Compositesv ia Containing Melamine Polyphosphate Modified Boron Nitride," Journal of Polymer Engin

eering 46 (2026): 154-163.
21. Z. Xuan, W. Xu, M. Zhao, et al., “Co-ZIF Modified Boron Nitride Co-Effecting Ammonium Polyphosphate: A Strategy for Improving the Flame Retardancy and Thermal Conductivity of Polyvinyl Alcohol,” Journal of Applied Polymer Science 143 (2026): e58039.
22. Z. Zhao, M. N. Prabhakar, Z. Zhang, et al., “A Comprehensive Review of Phytic Acid as a Bio-Based Flame Retardant for Polymer Composites,” Journal of Vinyl and Additive Technology 32 (2026): 390-409.
23. A. Bifulco and G. Malucelli, “Phytic Acid and Its Derivatives as Valuable Flame Retardants for Polymer Systems: Current State of the Art and Perspectives,” Polymers 18 (2026): 671.
24. B. Wang, S. Wei, L. Zhou, et al., “Phytic Acid-Iron Synergized Straw Cellulose-Based Polyurethane Biocomposite for Flame-Retardant Applications,” International Journal of Biological Macromolecules 339 (2026): 152005
25. Y. Cui, H. Jiang, Y. Hu, et al., “Phytic Acid/ADP Interfacial Assembly for Flame Retardancy and Self-Extinguishment in Cellulose Paper,” ACS Omega 323 (2026): 147199.
26. H. Chen, W. Zeng, J. Mei, et al., “Enhancing Flame Retardancy, Mechanical Strength, and Self-Healing Property of Waterborne Polyurethane via Diselenide and Modifying Al/Zn @Phytic Acid,” Chemical Engineering Journal531 (2026): 173962.
27. L. He, Z. Sui, Q. Zhang, et al., “Phytic Acid-Chitosan/Silicone Polyurethane Composite Coating: A Versatile Strategy for Flame-Retardant, Water-Repellent, and Antibacterial Hemp Cellulose Fabrics,” International Journal of Biological Macromolecules 361 (2026): 152022.
28. M. Guo, W. Wang, Z. Zhu, et al., “Phytic Acid-Bridged MXene/Fe-MOF Nanohybrids: A Dual Synergy for Enhanced Flame Retardancy, Smoke Suppression and Mechanical Properties in Poly(L-Lactic Acid),” Polymer 354 (2026): 129994.
29. C. Li, M. Cheng, R. Chen, et al., “The Research of a Novelty Bio-Based Flame Retardant Derived from the Synthetic Combination of Alkaline-Extracted Polymer Substances from Wastewater Sludge with Phytic Acid,” Journal of Environmental Management401 (2026): 128826.
30. M. Xiao, X. Jia, Y. Wang, et al., “Flame-Retardant Modification of Cotton Fabrics for Aviation Safety Applications: A Study on a Phytic Acid-Chitosan Nanocoating Based on Layer-by-Layer Self-Assembly Technology,” Reaction Chemistry & Engineering 48 (2026): 15120-15135.
31. W. Li, T. Ruan, Y. Yin, et al., “Fabrication and Performance Evaluation of Hydrophobic Flame-Retardant Coatings on Polyester Substrates via Phytic Acid and Siloxane,” Progress in Organic Coatings 213 (2026): 109914.
32. M. Hajibeygi and M. Heydari, “Enhanced Flame Retardancy and Thermal Stability of PLA via DOPO-Based Polyamide and Phytic Acid/PEI-Modified CaAl LDH: A Synergistic Approach Through Bulk and Coating Strategies,” Progress in Organic Coatings210 (2026): 109650.
33. S. Wang, Y. Yang, L. Zhang, et al., “Supramolecular Phytic Acid/Melamine Self-Assembly Coatings for Flexible Polyurethane Foam with Superior Flame Retardancy and Fire-Warning,” Journal of Applied Polymer Science 143 (2026): e70395.
34. J. Jiang, E. Deng, J. Hu, et al., “Bioengineered Chitosan Derivatives: Design, Multifun

ctionality and Flame Retardant Efficacy in Epoxy Resin – A Critical Review," Polymer De gradation and Stability 248 (2026): 112055.
35. X. Zhang, Y. K. Xu, B. Zhao, et al., "The Preparation, Properties and Flame Retardant Mechanism of Chitosan Oligosaccharide Bio-Based Flame-Retardant Polyester Fabrics," Pr ogress in Organic Coatings 210 (2026): 109738.
36. N. Sun, S. Liu, Q. Chen, et al., "Synergistic Enhancement of the Flame Retardancy, Mechanical Properties, and Thermal Insulation of Rigid Polyurethane Foam via a Boron-C ontaining Chitosan Derivative," ACS Applied Polymer Materials 8 (2026): 5446-5458.
37. Z. Yin, Y. Jiang, F. Meng, et al., "Nacre-Inspired Flame-Retardant Coating with a Bric k–Mortar Architecture Based on Bio-Based Chitosan/Gelatin and APP/MMT for Flexible P olyurethane Foam," ACS Applied Polymer Materials 8 (2026): 3312-3328.
38. L. Bai, W. Tan, Y. Tian, et al., "Preparation of Flame Retardant and Antibacterial Mul tifunctional Lyocell Fabric Based on Bio-Based Taurine-Chitosan Derivative," Polymer Degr adation and Stability 246 (2026): 111935.
39. G. Sharma, A. Dey, and K. Pal, "Bio-Based Chitosan-Al³⁺-Microcrystalline Cellulose Aerogel with Modified Surface Properties for Flame Retardancy, Thermal Insula tion and Sound Absorption Applications," Sustainable Materials and Technologies443 (2026) : e01948.
40. Z. Xu, P. Xing, Y. Pan, et al., "Sustainable Chitosan Composite Foams: Synergistic Hy droxyapatite Nanowires/Phytic Acid-Melamine Hybridization for Reliable Fire Warningand Efficient Flame Suppression," Carbohydrate Polymers381 (2026): 125137.
41. W. Wang, P. Liu, L. Zhang, et al., "Construction of an Eco-Friendly Intumescent Flam e Retardant with Bio-Based Chitosan-Phytic Acid for Enhancing the Flame Retardancy of PBAT," Reactive and Functional Polymers 222 (2026): 106682.
42. P. Li, Y. Rong, X. Zhang, et al., "Strategy to the Scaffold Effect of Polyester-Cotton Fabrics: A Fully Encapsulated Chitosan-Based Flame-Retardant Coating with IntegratedAnti bacterial and Recyclable Properties," International Journal of Biological Macromolecules 34 4 (2026): 150573.
43. K. Wu, C. Lei, W. Yang, et al., "Surface Modification of Boron Nitride by Reduced Graphene Oxide for Preparation of Dielectric Material with Enhanced Dielectric Constant a nd Well-Suppressed Dielectric Loss," Composites Science and Technology 134 (2016): 191-200.
44. C. V. S. Rosely, A. M. Joseph, A. Leuteritz, et al., "Phytic Acid Modified Boron Nitri de Nanosheets as Sustainable Multifunctional Nanofillers for Enhanced Properties of Poly(L -Lactide)," ACS Sustainable Chemistry & Engineering 8 (2020): 1868-1878.
45. T. Zhang, H. Yan, L. Shen, et al., "Chitosan/Phytic Acid Polyelectrolyte Complex: A Green and Renewable Intumescent Flame Retardant System for Ethylene–Vinyl Acetate Co polymer," Industrial & Engineering Chemistry Research 53 (2014): 19199-19207.
46. H. Jiang, Y. Xie, M. He, et al., "Highly Thermally Conductive and Flame-Retardant W aterborne Polyurethane Composites with 3D BNNS Bridging Structures via Magnetic Field Assistance," Nano-Micro Letters 17 (2025): 138.
47. W. Yan, J. Yu, M. Zhang, et al., "Enhanced Flame Retardancy of Epoxy Resin Contai ning a Phenethyl-Bridged DOPO Derivative/Montmorillonite Compound," Journal of Fire S ciences 36 (2018): 47-62.

48. K. A. Salmeia, J. Fage, S. Liang, et al., “An Overview of Mode of Action and Analytical Methods for Evaluation of Gas Phase Activities of Flame Retardants,” Polymers7 (2015): 504-526.
49. S. Yin, X. Ren, P. Lian, et al., “Synergistic Effects of Black Phosphorus/Boron Nitride Nanosheets on Enhancing the Flame-Retardant Properties of Waterborne Polyurethane and Its Flame-Retardant Mechanism,” Polymers 12 (2020): 1487.
50. Y. Zou, Y. Li, S. Bourbigot, et al.,. Determination of solid-phase reaction mechanism and chlorine migration behavior of co-pyrolyzing PVC–CaCO3 based polymer using temperature-dependent FTIR and XRD analysis. Polymer Degradation and Stability 193 (2021): 109741..
51. L. Yang, J. Guo, L. Zhang, et al., “Significant Improvement in the Flame Retardancy and Thermal Conductivity of the Epoxy Resin via Constructing a Branched Flame Retardant Based on SI-ATRP Initiated by Dopamine-Modified Boron Nitride,” Industrial & Engineering Chemistry Research 61 (2022): 8031-8042.
52. Y. Xie, C. Liu, Y. Wang, et al., “Waterborne Polyurethane Treated with Flame Retardant Based on Polydimethylsiloxanes and Boron Phenolic Resin for Improving the Char Residue and Anti-Dripping Performance,” Molecules 29 (2024): 5799.
53. A. Patti and D. Acierno, “Structure-Property Relationships of Waterborne Polyurethane (WPU) in Aqueous Formulations,”Journal of Vinyl and Additive Technology 29 (2023): 589-606.
54. Y. J. Lee, Y. La, O. S. Jeon, et al., “Effects of Boron Nitride Nanotube Content on Waterborne Polyurethane–Acrylate Composite Coating Materials,” RSC Advances 11 (2021): 12748-12756.
55. M. Demiral, “Strength in Adhesion: A Multi-Mechanics Review Covering Tensile, Shear, Fracture, Fatigue, Creep, and Impact Behavior of Polymer Bonding in Composites,”Polymers 17 (2025): 2600.
56. Y. Ding, L. Sun, J. Qu, et al., “Design and Synthesis of a Dual-DOPO-Based Flame Retardant: Performance Evaluation and Mechanistic Study in Waterborne Polyurethane Systems,” Progress in Organic Coatings 205 (2025): 109330.
57. Q. Zhang, Y. Sun, and Y. Liu, “Green Synthesis of Chitosan–Phytic Acid Polymers and Nanoparticles,” Industrial Crops and Products 199 (2023): 116747.
58. M. G. Rasul, A. Kiziltas, B. Arfaei, et al., “2D Boron Nitride Nanosheets for Polymer Composite Materials,” npj 2D Materials and Applications 5 (2021): 56.

Supplementary Files

This is a list of supplementary files associated with this preprint. Click to download.

- abstract.pdf
- supportinginformation.docx